14207

Cohesive Energy: The Intrinsic Dominant of Thermal Stability and Structural Evolution in Sn from Size Scales of Bulk to Dimer

C. C. Yang* and S. Li

School of Materials Science and Engineering, The University of New South Wales,
Sydney, NSW 2052, Australia

Size-dependent cohesive energy, $E_c(n)$, is the intrinsic dominant for thermal stability and structural evolution of materials, where n denotes the number of atoms in the material of a particular size. In this work, the $E_c(n)$ of Sn_n from the size scales of bulk ($n = \infty$) to dimer ($n = 2$) is investigated using nanothermodynamic models and ab initio density-functional theory (DFT) with the generalized gradient approximation. With the classification of material structural evolution caused by decreasing n, $E_c(n)$ could be divided into four regimes: (1) For nanoparticles with bulk crystallographic structures ($n \geq 1000$), $E_c(n)$ increases nonlinearly with the decrease of n. (2) For large-sized clusters with spherical-like structures ($35 < n < 1000$), $E_c(n)$ is proportional to $n^{-1/3}$. (3) For medium-sized clusters with prolate structures ($10 \leq n \leq 35$), $E_c(n)$ is size-independent. (4) For small-sized clusters with specific structures ($2 \leq n < 10$), $E_c(n)$ increases with decreasing n rapidly. In addition, the ground-state structures and size dependence of the highest-occupied and lowest-unoccupied molecular orbital gap in Sn_n ($n = 2-20$) clusters are also studied with DFT. The calculated and simulated results are in good agreement with experimental and other simulation results. The findings in this work may provide new insight into the fundamental understanding of the thermal stability in nanostructured and cluster-assembled materials.

1. Introduction

In last two decades, low-dimensional nanomaterials have been widely researched because of their unique electronic, magnetic, optic, catalytic, and thermodynamic properties, which are different substantially from their bulk properties.[1] As the size further decreases, there are only a few to several hundred atoms in a solid. This may result in instability of the crystalline structures because of the large surface/volume ratio and bond deficit.[2-4] In this size regime, the structures and properties of clusters are remarkably different from their counterparts in bulk and also in nanometer scales. Recently, this has become an important subject as the continuing miniaturization of electronic devices will make the minimal device features eventually reach the size regime of atomic clusters.[5] Moreover, the cluster-assembled materials also offer the attractive proposition to develop materials with tailored physicochemical properties.[6-10] To realize novel nanostructured or cluster-assembled materials associated with their potential technological applications in nanodevices, fundamental and challenging issues need to be addressed. For example, how do the structural arrangement of atoms and the electronic states of the system change with aggregation size increasing from single atom to bulk condensed matter? What are the determinants of the thermal stability in such nanocrystals and nanoclusters? On the other hand, cohesive energy $E_c(n)$ is defined as the difference between the average energy of the atoms in a solid and the isolated atoms, where n denotes the number of atoms in the materials. It is one of the most important physical parameters in quantifying the thermal stability of materials. For example, $E_c(n)$ determines the size dependence of a number of physicochemical properties in low-dimensional materials such as melting temperature, evaporation temperature, Debye temperature, critical temperature for ferromagnetic, ferroelectric, and superconductor transition, formation enthalpy, surface energy, interface energy, diffusion activation energy, vacancy formation energy, band gap energy, and thermal conductivity.[11-19] As a result, the investigation of $E_c(n)$ has become one of the most important topics in thermodynamics of solid-state materials.

In general, the structural evolution of materials can be divided into four regimes with decreasing n: (I) nanocrystals, (II) large-sized clusters, (III) medium-sized clusters, and (IV) small-sized clusters. Numerous experimental and theoretical efforts (nanothermodynamic modeling and computer simulations) have been implemented to investigate the $E_c(n)$ of materials in these four different regimes. In regime I, the $E_c(n)$ of Mo and W nanoparticles was obtained experimentally by measuring their oxidation enthalpies using a differential scanning calorimeter.[20] The results show that $E_c(n)$ increases with decreasing n, and this phenomenon has been explained by several thermodynamic models.[11,13,14,21] In regime II, the $E_c(n)$ of Si, Sn, and SnTe nanoclusters with $n < 1000$ was determined experimentally by a micromechanical calorimeter.[22-24] It is found that the $E_c(n)$ is proportional to $n^{-1/3}$, and the classic liquid droplet model (LDM)[25,26] was extended to elucidate this size-dependent phenomenon. In regimes III and IV, the experimental approaches and algorithms for improving accuracy have been widely used to investigate the ground-state structures and the thermal stability of various elementary and compound clusters.[2-10,27-48] These investigations have established a framework for further investigation of the structural evolution and thermal stability of materials. However, to date, there is a lack of a systematic investigation in the size-dependent $E_c(n)$ from the size scales of bulk to dimer. This has impeded the rapid development of nanostructured or cluster-assembled materials.

* To whom correspondence should be addressed. E-mail: ccyang@ unsw.edu.au. Fax: +61-2-93855956.

14208 *J. Phys. Chem. C, Vol. 113, No. 32, 2009*

Yang and Li

The position of semimetallic Sn in the elementary periodic table is between the semiconducting element Ge and metallic element Pb. Bulk Sn is metallic β-Sn with a body centered tetragonal structure at atmospheric pressure and temperature. It transforms into semiconducting α-Sn with a diamond structure upon decreasing the temperature below 286 K.[49] However, it was reported that medium- and small-sized Sn clusters have similar geometries to those found in Si and Ge clusters rather than in metal clusters.[30,31,33,34,36-40,42,44,45] These make it important to investigate the thermal stability and structural evolution of Sn nanoclusters. Moreover, the ion mobility measurements indicate that the melting temperature of Sn clusters with $10-30$ atoms could be at least 50 K higher than that of the bulk materials.[32] This is in contrast to which melting points are generally depressed by the size reduction to cluster level.[50,51] This abnormal superheating phenomenon may have paramount technological applications in the fabrication of nanodevices and has triggered enormous research efforts.

In this work, an approach was implemented to combine nanothermodynamics and ab initio density functional theory (DFT) to investigate the structural evolution and size-dependent $E_c(n)$ of Sn. The accuracy of the developed methodology is verified with available experimental data. The findings in this work may provide new insight into the fundamental understanding of the thermal stability and structural evolution of the materials with the size from bulk to dimer.

2. Methodology

The four regimes for the structural evolution of Sn from bulk to dimer are defined as (I) $n \geq 1000$, nanocrystals with the bulk crystallographic structures,[50] (II) $35 < n < 1000$, large-sized clusters with spherical-like structures,[23,24,51] (III) $10 \leq n \leq 35$, medium-sized clusters with prolate structures,[30,31,33,34,36-40,42,44-46] and (IV) $2 \leq n < 10$, small-sized clusters with specific structures.[29,34,35,38,41,42,46] The size-dependent $E_c(n)$ of Sn in these four size regimes is detailed in the following sections.

2.1. $E_c(n)$ of Nanoparticles with Spherical Structures. In regime I, only zero-dimensional nanoparticles, as a typical example, are investigated as the dimensionality effect is not the focus of this work. With the developed $E_c(D)$ function[15,17-19,21] for nanoparticles and the correlation of $D = hn^{1/3}$ (D and h are the cluster and atomic diameters, respectively), the $E_c(n)/E_c(\infty)$ function for the nanoparticles can be expressed as

$$E_c(n)/E_c(\infty) = \left(1 - \frac{1}{2n^{1/3} - 1}\right) \exp\left(-\frac{2S_b}{3R} \frac{1}{2n^{1/3} - 1}\right) \tag{1}$$

where $E_c(\infty)$ denotes the bulk cohesive energy, S_b is the bulk solid-vapor transition entropy of a crystal, and R is the ideal gas constant.

For $n \geq 1000$, $2n^{1/3} \gg 1$ and $\exp\{[-2S_b/(3R)]/(2n^{1/3} - 1)\} \approx 1 - [S_b/(3R)]n^{-1/3}$ with a first-order approximation. Therefore, eq 1 can be rewritten as

$$E_c(n)/E_c(\infty) \approx 1 - [S_b/(3R)]n^{-1/3} \tag{2}$$

2.2. $E_c(n)$ of Large-Sized Clusters with Spherical-Like Structures. In LDM, the $E_c(n)$ of Sn clusters is assumed to be the sum of energies contributed by $E_c(\infty)$ and surface energy γ with $E_c(n) = \chi[E_c(\infty) + \gamma] + (1 - \chi)E_c(\infty)$, where $\chi = n_s/n$ denotes the surface/volume ratio, and n_s is the surface atomic

number.[14,47,48,52] Thus, the $E_c(n)/E_c(\infty)$ in regime II can be obtained by

$$E_c(n)/E_c(\infty) = 1 + \gamma\chi/E_c(\infty) \tag{3}$$

The γ in eq 3 can be calculated with $\gamma = -[1 - (Z_s/Z_b)^{1/2}]E_c(\infty)$ according to the modified broken bond theory, where Z_s is the nearest-neighbor coordination number (CN) of the surface atoms, and Z_b is the bulk nearest-neighbor CN.[53] For Sn with a diamond structure and with the consideration of contribution to the total energy from the next-nearest-neighbor atoms to a surface atom,[16] $\gamma = -E_c(\infty)\{[1 - (Z_s/Z_b)^{1/2}] + \eta[1 - (Z_s'/Z_b')^{1/2}]\}/(1 + \eta)$, where η denotes the total bond strength ratio between the next-nearest neighbor and nearest neighbor, Z_s' and Z_b', the next-nearest-neighbor CNs correspond to Z_s and Z_b.[16] It is assumed that $3h$ is a critical diameter of the nanocluster with all atoms on its surface.[16] As a result, $\chi = 3h/D = 3n^{-1/3}$. From eq 3 and the expressions of γ and χ, we have

$$E_c(n)/E_c(\infty) = 1 - 3n^{-1/3}\{[1 - (Z_s/Z_b)^{1/2}] + \eta[1 - (Z_s'/Z_b')^{1/2}]\}/(1 + \eta) \tag{4}$$

2.3. $E_c(n)$ of Medium-Sized Clusters with Prolate Structures. The experimental and computer simulation results demonstrated that the Sn_n clusters ($10 \leq n \leq 35$) grow with the prolate shape with all atoms located on the surface.[30,37-39,42,44,45] From our assumption of $\chi = 3n^{-1/3}$, $\chi = 1$ for a cluster with $n \leq 27$. This is approximately consistent with the above findings that $\chi = 1$ for $10 \leq n \leq 35$. In this case, from eq 4 and $\chi = 1$ in regime III, the $E_c(n)/E_c(\infty)$ function can be expressed as

$$E_c(n)/E_c(\infty) = 1 - \{[1 - (Z_s/Z_b)^{1/2}] + \eta[1 - (Z_s'/Z_b')^{1/2}]\}/(1 + \eta) \tag{5}$$

2.4. $E_c(n)$ of Small-Sized Clusters with Specific Structures. In regime IV, ab initio DFT calculations on Sn_n ($n = 2-20$) clusters are implemented by using an all electron DMOL[3] code with a double numerical basis, including d-polarization function (DND).[54,55] Note that the simulation results of Sn_n ($n = 10-20$) clusters are utilized to (1) verify the accuracy of eq 5 because of the lack of experimental data on $E_c(n)$ in regime III and (2) reveal the structural evolution from $n = 2-9$ to $n = 10-20$. The exchange-correlation interaction was treated within the generalized gradient approximation (GGA) of the revised Perdew-Burke-Ernzerhof (RPBE) function,[56] which is advantageous in calculating the cohesive energies for small molecules.[47,57] Self-consistent field (SCF) electronic structure calculations were conducted with a convergence criterion of 1.0×10^{-6} Ha (1 Ha = 27.2114 eV) on the total energy. Bulk Sn and Sn_n clusters with $n = 2-20$ were optimized with a convergence tolerance of 1.0×10^{-5} Ha of energy, 0.002 Ha/Å of maximum force, and 0.005 Å of maximum displacement. The smearing technique with a value of 0.001 Ha was used for all structures in the simulations. In all cases, spin polarization was introduced. The accuracy of the present DFT computational methodology is verified by a benchmark calculation on bulk Sn and Sn dimer. Moreover, the electronic property of the highest-occupied and lowest-unoccupied molecular orbital (HOMO-LUMO) gap $E_g(n)$ was also investigated.
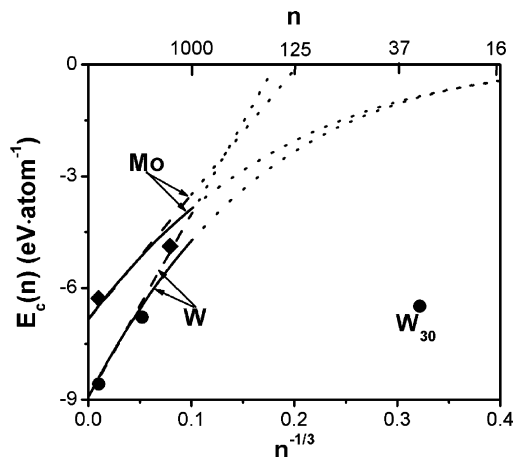
Cohesive Energy

J. Phys. Chem. C, Vol. 113, No. 32, 2009 **14209**

Figure 1. $E_c(n)$ of Mo and W nanoparticles. Solid and dashed lines denote model predictions from eqs 1 and 2, respectively, for $n \geq 1000$, where the extension parts ($n < 1000$) are shown as the dotted lines. Symbols ◆ and ● are experimental data of Mo and W, respectively.[20]

3. Results and Discussion

Figure 1 plots the calculations from eqs 1 and 2 as well as the experimental results of $E_c(n)$ for Mo and W nanoparticles, which are the only available experimental data for the nanocrystals found in the open literature. The related parameters used in the modeling are for Mo, $E_c(\infty) = -6.842$ eV atom^{-1} and $S_b = 122.15$ J mol$^{-1} \cdot$K^{-1} and for W, $E_c(\infty) = -8.929$ eV atom^{-1} and $S_b = 137.27$ J mol^{-1} K^{-1}.[58] It is discernible that the calculation results of $E_c(n)$ increase with decreasing n, indicating the instability of nanocrystals compared with the corresponding bulk crystals. This observation is in good agreement with the experimental data of Mo and W nanoparticles where the number of atoms is more than 1000. It demonstrates the accuracy of the developed model. The surface/volume ratio increases with the reduction of the nanoparticle size or atomic number n, resulting in a higher energetic state of surface atoms and thus enhancing the cohesive energy.[11–19,21] From Figure 1, it can be seen that the results from eqs 1 and 2 are overlapped when $n^{-1/3} < 0.05$ or $n > 8000$, while they start to separate in the range of $1000 < n < 8000$. It shows that eq 2 is a good approximation of eq 1 for the nanoparticles with large size. However, eq 2 obeys the thermodynamic rule of low-dimensional materials in which the alternation of the size-dependent quantity is associated with the surface/volume ratio, or $n^{-1/3}$.[11,13,14] This further supports the notion that the physicochemical properties of nanocrystals are most likely affected by severe bond dangling, which is induced by the crystal size reduction in nanometer scale. Moreover, it is noted that there is a large deviation between the experimental $E_c(n)$ value of the W$_{30}$ ($n = 30$) nanocluster and calculation results from the eqs 1 and 2. This is because the developed models of eqs 1 and 2 are only suitable for crystalline structural materials with the consideration of a continuous medium. Although eqs 1 and 2 are suitable for mesoscopic particles with thousands of atoms, they are not applicable to the clusters with less numbers of atoms as shown in the dotted lines in Figure 1. This is caused by the structural revolution with the collapse of the long-range-ordered lattice structures in nanoparticles and the heavily reconstructed geometries of atomic clusters.

Figure 2 plots the calculation from eq 4 and the experimental results of $E_c(n)$ for Sn$_n$ nanoclusters with $n < 1000$. The related parameters used in the modeling are $E_c(\infty) = -3.14$ eV atom^{-1},[59] $Z_s = 3$, $Z_b = 4$, $Z_s' = 6$, $Z_b' = 12$, and $\eta = 3/10$.[16]
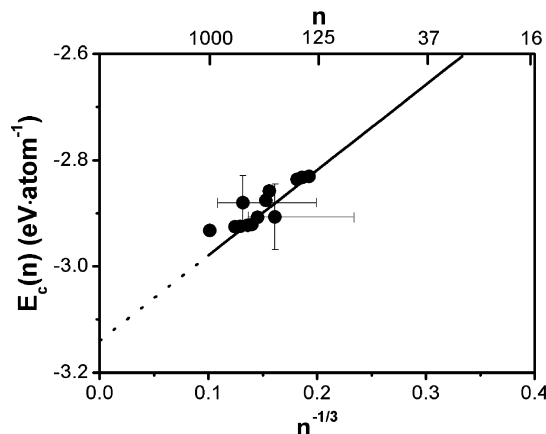

Figure 2. $E_c(n)$ of large-sized Sn clusters. Solid line denotes the model prediction from eq 4 for $n < 1000$, where the extension part ($n \geq 1000$) is shown as the dotted line. Symbols ● are experimental data.[23,24]
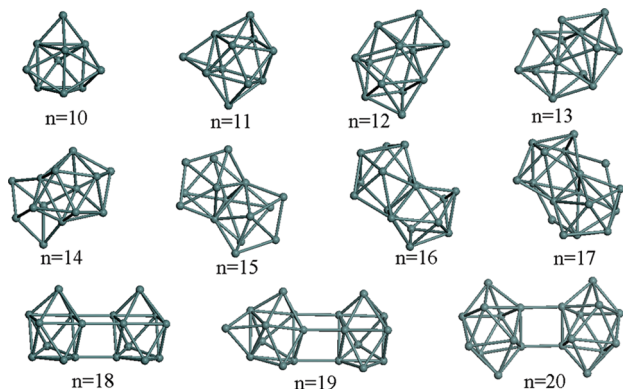
TABLE 1: Simulation (GGA-RPRE) and Experimental Results of Lattice Constant a (or Bond Length) and Cohesive Energy of Bulk Sn and Sn Dimer

		experimental	GGA-RPBE
bulk Sn	a (nm)	0.649[59]	0.6753
	$E_c(\infty)$ (eV atom^{-1})	−3.14[59]	−2.998
Sn dimer	a (nm)	0.275[28]	0.2856
	$E_c(2)$ (eV atom^{-1})	−0.964 ± 0.047[27]	−1.182

The results show that the $E_c(n)$ increases with decreasing n, exhibiting a linear relationship between $E_c(n)$ and $n^{-1/3}$. It indicates that the reduction of n depresses the thermal stability of the nanoclusters. This calculation result is consistent with the experimental data, demonstrating the accuracy of the developed model. Note that γ is size-independent, similar to LDM approach.[25,26] In fact, the modified broken bond theory could be rewritten as $\gamma(n) = -\{1 - [Z_s(n)/Z_b]^{1/2}\}E_c(n)$ for nanoclusters. With n decreasing, $Z_s(n)$ and the absolute value of $E_c(n)$ decrease, resulting in $\gamma(n) \approx \gamma(\infty)$. This has recently been verified with the ab initio DFT calculations for Ag nanoclusters.[48] The consistency between the calculations results from eq 4 and the experimental data of $E_c(n)$ in Sn clusters also implies that the size-independent γ or $\gamma(n) \approx \gamma(\infty)$ is a good approximation. Similar to Figure 1, the dotted line in Figure 2 indicates that eq 4 is not applicable for nanoparticles with $n \geq 1000$.

Furthermore, the accuracy of the GGA-RPBE computational scheme is verified by a benchmark calculation on bulk Sn and Sn dimer. The corresponding simulation results are listed in Table 1. As shown in Table 1, the $E_c(\infty)$ value of bulk Sn with the diamond crystallographic structure obtained from GGA-RPBE matches the experimental data with deviation of 4.52%, while the $E_c(2)$ value is a little underestimated. Moreover, the lattice constant of bulk Sn and bond length of Sn$_2$ determined by GGA-RPBE are also consistent with experimental data within the accuracy of 4.05%. Therefore, we believe that the GGA-RPBE approach can be utilized to simulate the structures and properties of Sn nanoclusters.

Although the experimental and theoretical approaches are different,[28,29,34,35,37,38,42,46] the results of the lowest energy structure and bonding state for each Sn nanocluster with these approaches are consistent. Note that a large number of isomers have been considered for each cluster in these approches. In order to simplify the calculation, only the lowest energy structures reported in the open literature were selected as the initial geometries of Sn clusters in our simulations. Through
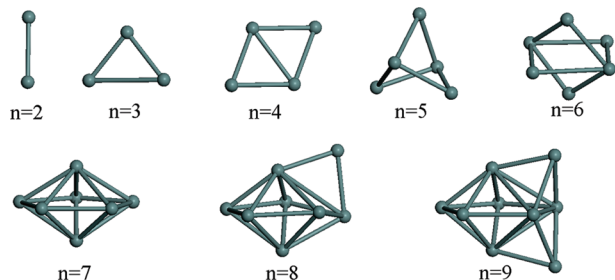
Figure 3. Structures of small-sized Sn_n clusters with $n = 2-9$.

Figure 4. Structures of medium-sized Sn_n clusters with $n = 10-20$.

TABLE 2: Simulation (GGA-RPBE) and Experimental Results of $E_c(n)$ and $E_g(n)$ in Sn_n Nanoclusters ($n = 2-20$)

n	$E_c(n)$ (eV atom^{-1})	$E_c(n)$ (eV atom^{-1}) (experimental)	$E_g(n)$ (eV)	$E_g(n)$ (eV) (experimental)[33]	$E_g(n)$ (eV) (experimental)[45]
2	−1.182	−0.964 ± 0.047[27]	0.446		
3	−1.663	−1.664 ± 0.059[27]	0.872		
4	−2.092	−1.947 ± 0.036[35]	1.078	0.9943	0.93 ± 0.07
5	−2.260	−2.056 ± 0.046[35]	1.527	0	0.17 ± 0.06
6	−2.424	−2.335 ± 0.048[35]	1.5	0.4213	0.43 ± 0.06
7	−2.533	−2.439 ± 0.055[35]	1.493	1.4289	1.25 ± 0.07
8	−2.468		0.957	0.1974	0.16 ± 0.06
9	−2.530		1.303	0.218	0.22 ± 0.05
10	−2.606		1.487	0.2033	0.16 ± 0.05
11	−2.546		0.752	0.3005	0.32 ± 0.05
12	−2.543		0.799	0.7969	0.25 ± 0.06
13	−2.567		0.811	0.3388	0.40 ± 0.05
14	−2.611		1.351	0.4787	0.34 ± 0.05
15	−2.612		0.718	0.3933	0.38 ± 0.05
16	−2.612		1.246	0.6334	0.67 ± 0.05
17	−2.570		0.89	0.6835	0.64 ± 0.05
18	−2.621		0.521	0.5804	0.61 ± 0.05
19	−2.607		0.554	0.4125	0.35 ± 0.06
20	−2.626		0.71	0.4949	0.48 ± 0.05

the optimization with GGA-RPBE, the groud-state structures of the Sn_n clusters for $n = 2-9$ and $n = 10-20$ can be obtained as shown in Figures 3 and 4, respectively. From Figures 3 and 4, several interesting features can be found: (1) The equilibrium structures of Sn nanoclusters diverge significantly from those of the corresponding crystalline fragments due to severe broken bonds. (2) For $n \leq 7$, the Sn_n clusters share similar structures with Si and Ge clusters, which are consistent with the experimental results.[30,31,34,36−38,46] (3) The equilibrium geometries of Sn clusters undergo transitions from specific structures for $n = 2-9$ to the prolate geometry at $n = 10$, showing the same trends of Si and Ge clusters.[30,37,38,46] It is evident that the ground-state structures of Sn clusters are in a line with Si and Ge clusters rather than the typical metal clusters. Moreover, recent experimental and simulation results indicate that the ground-state geometries of Pb_n clusters possess similar structures as those of Si, Ge, and Sn clusters when $n \leq 7$.[60] However, the transition toward close-packed geometries has been observed for Pb_n clusters when $n = 8-10$. From $n = 11$, Pb_n clusters prefer close-packed and near-spherical structures rather than the prolate geometries. This growth pattern is standard for the clusters of typical metals. As a result, the transition of the bonding nature from covalent to metallic in the group of IV-A clusters occurs between Sn and Pb. This is different from that in the bulk elements.[33,37,39,42]

The simulated $E_c(n)$, HOMO−LUMO gap $E_g(n)$, and experimental results are summarized in Table 2. Note that there is no experimental data of $E_c(n)$ in the size regime of $n > 7$ due to the limitation and difficulty of the experimental techniques.[3] It is known that the second difference of total energies, $\Delta_2 E(n) = E(n + 1) + E(n - 1) - 2E(n)$, is also a sensitive physical parameter associated with the thermal stability of the clusters, where $E(n)$ is the total energy of Sn clusters.[38,42] Figure 5 shows the $\Delta_2 E(n)$ of Sn clusters as a function of n with $n = 3-19$, where the $E(n)$ values are obtained from our simulations. As shown in Figure 5, the maxima of $\Delta_2 E(n)$ appear at $n = 4, 7, 10, 14, 16,$ and 18. The clusters with these particular numbers

of atoms are called "magic clusters", which is defined as the cluster formed with a well-defined numbers of atoms spontaneously.[6] It indicates that these clusters are more stable than their neighboring clusters, which is consistent with experimental and other computer simulation results.[31,38,42] Figure 6 shows the $E_g(n)$ of Sn_n clusters ($n = 2-20$) from our simulation, experimental results, and also other simulation results. It is found that the $E_g(n)$ values of small- and medium-sized Sn clusters oscillate and gradually decrease with increasing n. Although the $E_g(n)$ in our simulation is overestimated, the size-dependent trend is consistent with the experimental data.[33,45] Moreover, as shown in Figure 6, the local maxima of $E_g(n)$ from our simulation appear at $n = 5-7, 10, 14,$ and 16, which suggests the pronounced stability of the corresponding clusters. This is approximately consistent with experimental results ($n = 4, 7, 12, 16,$ and 17, or $n = 4, 7,$ and $16-18$)[33,45] and other simulation results ($n = 6, 7, 10,$ and 12, or $n = 5-7, 9, 10, 14, 16,$ and $18-20$, or $n = 3, 5-7, 9, 10, 14,$ and 16).[34,38,42] Further simulation works will be implemented to investigate larger Sn_n clusters with $n > 20$ to reveal their bonding nature and stability.

Figure 7 shows the simulation and experimental results of $E_c(n)$ for Sn nanoclusters with $n = 2-7$. It is discernible that the calculated $E_c(n)$ increases rapidly with decreasing n, which is in good agreement with the experimental data with a discrepancy less than 0.22 eV. Figure 8 plots the calculation
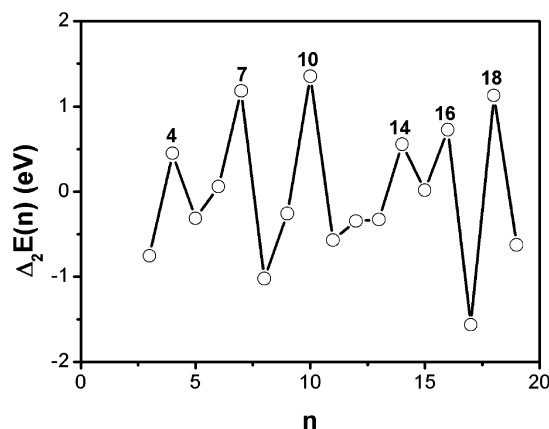
Figure 5. $\Delta_2 E(n)$ of Sn_n clusters with $n = 3-19$, where the magic clusters are marked with numbers. Solid lines are guides for the eyes.
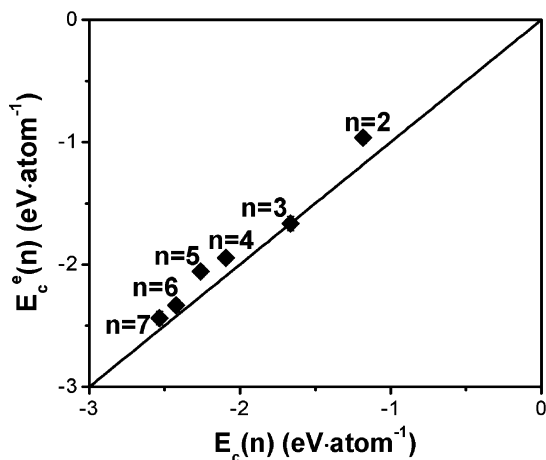
Cohesive Energy

J. Phys. Chem. C, Vol. 113, No. 32, 2009 **14211**

Figure 7. $E_c^e(n) - E_c(n)$ of small-sized Sn$_n$ clusters with $n = 2-7$, where $E_c^e(n)$[27,35] and $E_c(n)$ are experimental and our simulation results, respectively.
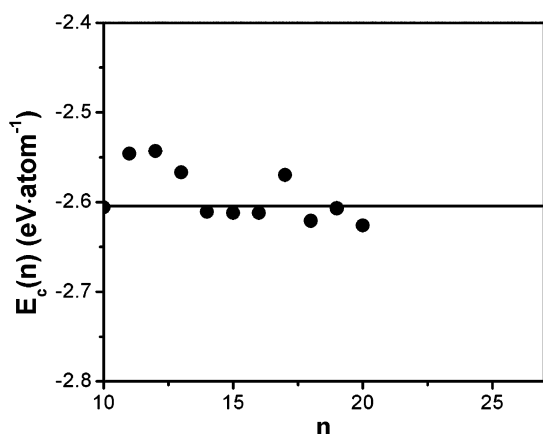

Figure 8. $E_c(n)$ of medium-sized Sn$_n$ clusters with $n = 10-27$. Solid line denotes the model prediction from eq 5. Symbols ● are our simulation results.

results from eq 5 and our simulation results of $E_c(n)$ for Sn nanoclusters with $n = 10-27$. It is found that the $E_c(n)$ values are almost size-independent in this size regime. This demonstrates the similarity of our model prediction, and simulation. $E_c(n) < E_c(\infty)$ was even reported for some Sn$_n$ clusters ($n = 6-13$) using a first-principles study within the local density approximation (LDA).[34] It is believed that LDA underestimates
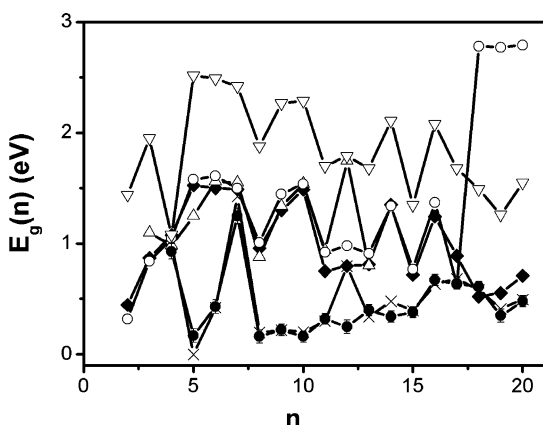

Figure 6. $E_g(n)$ of Sn$_n$ clusters with $n = 2-20$. Symbols ◆ are simulation results, ×[33] and ●[45] are experimental data, and △,[34] ○,[38] and ▽[42] are other simulation results. Solid lines are guides for the eyes.
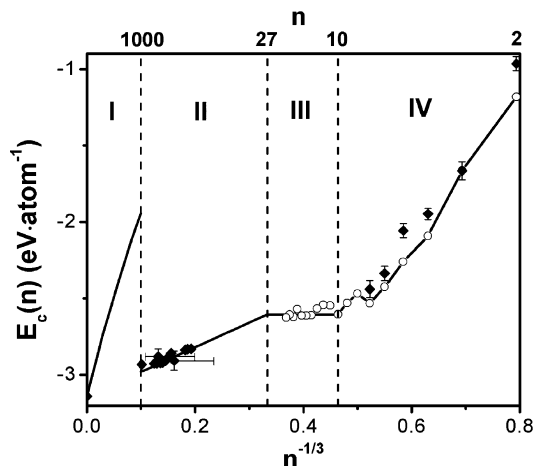

Figure 9. Summary of $E_c(n)$ in Sn. Solid lines in regimes I, II, and III denote the model predictions from eqs 1, 4, and 5, respectively. The symbols ◆[23,24,27,35,59] and ○ are experimental and our simulation results, respectively. Solid lines in regime IV are guides for the eyes. Dashed lines are used to divide different regimes.

the cohesive energy of small molecules, while GGA gives $E_c(n)$ with much higher accuracy.[42] As previously mentioned, an abnormal superheating of the medium-sized Sn$_n$ clusters ($n = 10-30$) has been observed experimentally.[32] It exhibits an opposite behavior as the melting point depression observed in Sn nanoparticles and large-sized Sn clusters.[50,51] Such a superheating phenomenon has been verified by experimental and theoretical studies for medium- and small-sized IV-A clusters.[39-41,43,44] However, the underlying mechanism is still unclear. We believe that the origins of the observed superheating for medium- and small-sized clusters are different. For the medium-sized Sn clusters, their low $E_c(n)$ and heavily reconstructed geometries may be the main mechanisms to cause the abnormal elevation of the melting points. As shown in Figure 8, $E_c(n) \approx -2.60$ eV atom^{-1}, which is only 17% higher than the $E_c(\infty)$ value (-3.14 eV·atom^{-1}), indicating that the bonds were strengthened in these clusters. Moreover, the direct transition of Sn clusters from prolate to near-spherical geometries occurs in the size range of $n = 35-65$.[30,32,37-39,42,44,45] In the small-sized regime, the heavily reconstructed geometries and the large number of dangling bonds may be responsible for the superheating of IV-A elements. The superheating of nanoclusters is a complex phenomenon and needs to be investigated in future.

The four regimes of structural evolution and size-dependent $E_c(n)$ of Sn are summarized in Figure 9, where $S_b = 100.87$ J mol^{-1} K^{-1} is used in eq 1.[58] Note that the calculated $E_c(n)$ values of Sn in regimes I and II are discontinuous, which may be caused by the collapse of the long-range-ordered crystallographic structure in nanoparticles and the heavily reconstructed geometries of atomic clusters. To the best of our knowledge, this may be the first systematic investigation of the size-dependent $E_c(n)$ of materials. Further experimental investigations will be implemented to reveal the correlation between the size, structures, and $E_c(n)$ for the clusters in the size regimes of I and III. In addition, the studies on IV-A clusters are just beginning because some fundamental issues, such as cluster growth kinetics and nonequilibrium effects are still unresolved. In order to understand the structural and property evolution from a single atom to condensed matter, the studies of larger clusters containing dozens or hundreds of atoms and even nanoparticles in several nanometers are required. With ever-increasing

computer power and the advance of experimental techniques, the challenges in this work will be overcome in the next few years.

4. Conclusions

An investigation with nanothermodynamics and ab initio DFT was implemented to reveal the intrinsic dominant of thermal stability and structural evolution from bulk Sn to dimer. The results show that size-dependent cohesive energy $E_c(n)$ plays an important role in determining these factors. The results present the following: (1) The $E_c(n)$ of Sn increases with decreasing n, except for $10 \leq n \leq 35$. (2) The size-independent $E_c(n)$ of Sn nanoclusters in the regime of $10 \leq n \leq 35$ was caused by their particular prolate structures. (3) The surface/volume ratio is the determinant of the size and structure dependence of $E_c(n)$ in nanocrystals and nanoclusters. (4) The size-independent surface energy is a good approximation for the clusters with large size ($35 < n < 1000$). (5) The GGA-RPBE scheme can present a good descreption of Sn. (6) The origins of the abnormal superheating observed in Sn and other IV-A elements are different for medium- and small-sized clusters.

References and Notes

(1) Gleiter, H. *Acta Mater.* **2000**, *48*, 1.

(2) Brown, W. L.; Freeman, R. R.; Raghavachari, K.; Schlüter, M. *Science* **1987**, *235*, 860.

(3) Jarrold, M. F. *Science* **1991**, *252*, 1085.

(4) Honea, E. C.; Oğura, A.; Murray, C. A.; Rağhavachari, K.; Sprenğer, W. O.; Jarrold, M. F.; Brown, W. L. *Nature* **1993**, *366*, 42.

(5) Ho, K.-M.; Shvartsburg, A. A.; Pan, B.; Lu, Z.-Y.; Wang, C.-Z.; Wacker, J. G.; Fye, J. L.; Jarrold, M. F. *Nature* **1998**, *392*, 582.

(6) Seifert, G. *Nat. Mater.* **2004**, *3*, 77.

(7) Kasuya, A.; Sivamohan, R.; Barnakov, Y. A.; Dmitruk, I. M.; Nirasawa, T.; Romanyuk, V. R.; Kumar, V.; Mamykin, S. V.; Tohji, K.; Jeyadevan, B.; Shinoda, K.; Kudo, T.; Terasaki, O.; Liu, Z.; Belosludov, R. V.; Sundararajan, V.; Kawazoe, Y. *Nat. Mater.* **2004**, *3*, 99.

(8) Yoo, S.; Zhao, J.; Wang, J.; Zeng, X. C. *J. Am. Chem. Soc.* **2004**, *126*, 13845.

(9) Gruene, P.; Rayner, D. M.; Redlich, B.; van der Meer, A. F. G.; Lyon, J. T.; Meijer, G.; Fielicke, A. *Science* **2008**, *321*, 674.

(10) Claridge, S. A.; Castleman, A. W., Jr.; Khanna, S. N.; Murray, C. B.; Sen, A.; Weiss, P. S. *ACS Nano* **2009**, *3*, 244.

(11) Qi, W. H.; Wang, M. P.; Zhou, M.; Hu, W. Y. *J. Phys. D: Appl. Phys.* **2005**, *38*, 1429.

(12) Liang, L. H.; Yang, G. W.; Li, B. W. *J. Phys. Chem. B* **2005**, *109*, 16081.

(13) Sun, C. Q. *Prog. Solid State Chem.* **2007**, *35*, 1.

(14) Vanithakumari, S. C.; Nanda, K. K. *J. Phys. Chem. B* **2006**, *110*, 1033.

(15) Yang, C. C.; Li, S. *Phys. Rev. B* **2007**, *75*, 165413.

(16) Jiang, Q.; Lu, H. M. *Surf. Sci. Reports* **2008**, *63*, 427.

(17) Jiang, Q.; Yang, C. C. *Curr. Nanosci.* **2008**, *4*, 179.

(18) Yang, C. C.; Armellin, J.; Li, S. *J. Phys. Chem. B* **2008**, *112*, 1482.

(19) Yang, C. C.; Li, S. *J. Phys. Chem. C* **2008**, *112*, 2851.

(20) Kim, H. K.; Huh, S. H.; Park, J. W.; Jeong, J. W.; Lee, G. H. *Chem. Phys. Lett.* **2002**, *354*, 165.

(21) Jiang, Q.; Li, J. C.; Chi, B. Q. *Chem. Phys. Lett.* **2002**, *366*, 551.

(22) Bachels, T.; Schäfer, R. *Chem. Phys. Lett.* **2000**, *324*, 365.

(23) Bachels, T.; Schäfer, R.; Güntherodt, H.-J. *Phys. Rev. Lett.* **2000**, *84*, 4890.

(24) Schäfer, R. *Z. Phys. Chem.* **2003**, *217*, 989.

(25) Becker, R.; Döring, W. *Ann. Phys.* **1935**, *24*, 719.

(26) Burton, J. J.; Briant, C. L. *Adv. Colloid Inter. Sci.* **1977**, *7*, 131.

(27) Gingerich, K. A.; Desideri, A.; Cocke, D. L. *J. Chem. Phys.* **1975**, *62*, 731.

(28) Bondybey, V. E.; Heaven, M.; Miller, T. A. *J. Chem. Phys.* **1983**, *78*, 3593.

(29) Jackson, P.; Dance, I. G.; Fisher, K. J.; Willett, G. D.; Gadd, G. E. *Int. J. Mass Spectrom. Ion Proc.* **1996**, *157/158*, 329.

(30) Shvartsburg, A. A.; Jarrold, M. F. *Phys. Rev. A* **1999**, *60*, 1235.

(31) Yoshida, S.; Fuke, K. *J. Chem. Phys.* **1999**, *111*, 3880.

(32) Shvartsburg, A. A.; Jarrold, M. F. *Phys. Rev. Lett.* **2000**, *85*, 2530.

(33) Negishi, Y.; Kawamata, H.; Nakajima, A.; Kaya, K. *J. Electron Spectrosc. Relat. Phenom.* **2000**, *106*, 117.

(34) Lu, Z.-Y.; Wang, C.-Z.; Ho, K.-M. *Phys. Rev. B* **2000**, *61*, 2329.

(35) Meloni, G.; Schmude, R. W., Jr.; Kingcade, J. E., Jr.; Gingerich, K. A. *J. Chem. Phys.* **2000**, *113*, 1852.

(36) Jo, C.; Lee, K. *J. Chem. Phys.* **2000**, *113*, 7268.

(37) Shvartsburg, A. A.; Hudgins, R. R.; Dugourd, P.; Jarrold, M. F. *Chem. Soc. Rev.* **2001**, *30*, 26.

(38) Majumder, C.; Kumar, V.; Mizuseki, H.; Kawazoe, Y. *Phys. Rev. B* **2001**, *64*, 233405.

(39) Joshi, K.; Kanhere, D. G.; Blundell, S. A. *Phys. Rev. B* **2002**, *66*, 155329.

(40) Joshi, K.; Kanhere, D. G.; Blundell, S. A. *Phys. Rev. B* **2003**, *67*, 235413.

(41) Chuang, F.-C.; Wang, C. Z.; Öğüt, S.; Chelikowsky, J. R.; Ho, K. M. *Phys. Rev. B* **2004**, *69*, 165408.

(42) Majumder, C.; Kumar, V.; Mizuseki, H.; Kawazoe, Y. *Phys. Rev. B* **2005**, *71*, 035401.

(43) Breaux, G. A.; Neal, C. M.; Cao, B.; Jarrold, M. F. *Phys. Rev. B* **2005**, *71*, 073410.

(44) Krishnamurty, S.; Joshi, K.; Kanhere, D. G.; Blundell, S. A. *Phys. Rev. B* **2006**, *73*, 045419.

(45) Cui, L.-F.; Wang, L.-M.; Wang, L.-S. *J. Chem. Phys.* **2007**, *126*, 064505.

(46) Schäfer, S.; Assadollahzadeh, B.; Mehring, M.; Schwerdtfeger, P.; Schäfer, R. *J. Phys. Chem. A* **2008**, *112*, 12312.

(47) Liu, W.; Liu, D.; Zheng, W. T.; Jiang, Q. *J. Phys. Chem. C* **2008**, *112*, 18840.

(48) Liu, D.; Lian, J. S.; Jiang, Q. *J. Phys. Chem. C* **2009**, *113*, 1168.

(49) Burgers, W. G.; Groen, L. J. *Discuss. Faraday Soc.* **1957**, *23*, 183.

(50) Lai, S. L.; Guo, J. Y.; Petrova, V.; Ramanath, G.; Allen, L. H. *Phys. Rev. Lett.* **1996**, *77*, 99.

(51) Bachels, T.; Güntherodt, H.-J.; Schäfer, R. *Phys. Rev. Lett.* **2000**, *85*, 1250.

(52) Tománek, D.; Mukherjee, S.; Bennemann, K. H. *Phys. Rev. B* **1983**, *28*, 665.

(53) Desjonquères, M. C.; Spanjaard, D. *Concepts in Surface Physics*, Springer Series in Surface; Springer: Berlin, Germany, 1993; Vol. 30.

(54) Delley, B. *J. Chem. Phys.* **1990**, *92*, 508.

(55) Delley, B. *J. Chem. Phys.* **2000**, *113*, 7756.

(56) Hammer, B.; Hansen, L. B.; Nørskov, J. K. *Phys. Rev. B* **1999**, *59*, 7413.

(57) Zhang, Y.; Yang, W. *Phys. Rev. Lett.* **1998**, *80*, 890.

(58) Web Elements Periodic Table. http://www.webelements.com/.

(59) Kittel, C. *Introduction to Solid State Physics*, 7th ed., John Wiley & Sons: New York, 1996, p 57.

(60) Rajesh, C.; Majumder, C.; Rajan, M. G. R.; Kulshreshtha, S. K. *Phys. Rev. B* **2005**, *72*, 235411, and references therein.